ADVANCED MATERIALS TECHNOLOGIES
www.advmattechnol.de

Wireless Human Motion Detection with a Highly Sensitive Wearable Pressure Sensing Technology

Jinli Yan, Jie Liu, Qing Qu, Xinjian Chen, Jian Liu, and Baoqing Nie**

Wireless flexible sensing devices using inductive-capacitive (LC) resonator-enabled transmission technologies are attractive in the areas of human motion detection, health inspection, and implantable medical devices. However, challenges remain in LC-based wireless sensing devices, including low device sensitivity/resolution and slow signal readout speed based on sweeping excitation frequencies. Herein, an LC resonator-based wireless pressure sensing technology (LC-WPS) is proposed for flexible contact pressure measurements in a real-time manner. It includes a fully flexible passive LC pressure sensor and a signal-reading circuit for wireless communication with the sensor and real-time data processing. The passive sensor detects external pressure by the changes in resonant frequency. Importantly, by optimizing the design of the LC resonator in the sensor, the LC-WPS converts the pressure-dependent resonant frequency into circuit output voltage to a great extent, achieving a high sensitivity (1.23×10^{-2} kPa^{-1}) and resolution (54 Pa) within a pressure range of 0–15 kPa. In addition, the LC-WPS utilizes a single operating frequency (i.e., 13.56 MHz) instead of sweeping the operating frequencies to identify the sensor resonant frequency, featuring fast and real-time data analysis and processing. Real-time monitoring of human motions, such as laryngeal movement, neck bending and wrist rotation, is demonstrated, verifying the applicability of the LC-WPS in the fields of wearable medical care and sports biomechanics.

1. Introduction

The development of flexible sensors in the fields of augmented reality (AR) increasingly raises the bar on device performance, such as sensitivity, flexibility, integration, and dimensional miniaturization.[1] Wireless flexible sensing systems are attractive because they can combine the functions of information sensing, data acquisition, processing and analysis, and wireless communication in a concise platform.[2] Javey et al. proposed an electrochemical sensor array equipped with Bluetooth technology for the measurements of sweat metabolites, electrolytes, and skin temperature.[3] Although their device identified multiple biomarkers in sweat, it was still built on rigid circuit components such as IC chips and batteries, which may limit its applications in those scenarios requiring improved flexibility and miniaturization.[4] Another approach for wireless sensing is available by integrating near-field communication (NFC) technology. Rogers et al. designed an ultrathin flexible sensor based on the NFC protocol to monitor the vital signs of neonates, such as blood pressure, skin temperature, respiration rate and heart rate.[5] Their design allowed for removal of the external power supply and unnecessary wires, thus minimizing wire breakage or wire entanglement on the skin of neonates. However, NFC-based passive sensing technologies still rely on rigid semiconductor circuits to harvest energy from the radio frequency field.[5,6]

In the near-field regime, one strategy to design chip-free wireless sensors relies on electromagnetic induction between the loop antenna/coil in an inductance-capacitance (LC) resonator. The passive sensor with the LC architecture features a unique self-resonator frequency tunable by any external stimuli altering the inductance or capacitance values. This design allows for physically separating the sensor and the signal-reading circuit and offers several advantages, including simplified architecture, ease of miniaturization, and full flexibility of the sensor node.[7] Researchers have demonstrated a variety of applications based on this strategy, such as plantar pressure measurement,[2a] invasive intraocular pressure detection,[7d] and arterial blood flow measurement.[8] In addition to the self-resonant frequency, external stimuli can be measured by the changes in the quality factor Q of the LC structure. A recent report introduced a stretchable sensing tag with an LC resonator and a resistive load to monitor human pulse, breath, and body movement in correlation to

J. Yan, J. Liu, X. Chen, B. Nie
School of Electronic and Information Engineering Soochow University
Suzhou, Jiangsu 215006, People's Republic of China
E-mail: qixinbq@suda.edu.cn
Q. Qu, J. Liu
Institute of Functional Nano and Soft Materials
Jiangsu Key Laboratory for Carbon-Based Functional Materials and Devices Soochow University
Suzhou, Jiangsu 215123, People's Republic of China
E-mail: jliu@suda.edu.cn
X. Chen
State Key Laboratory of Radiation Medicine and Protection Soochow University
Suzhou, Jiangsu 215123, People's Republic of China
The ORCID identification number(s) for the author(s) of this article can be found under https://doi.org/10.1002/admt.202201936

DOI: 10.1002/admt.202201936

Q variations.[9] This design can bypass rigid silicon chips in the sensor tag, allowing for improved wearability of the device. However, most LC circuits in previous studies had to sweep the operating frequencies every time in response to the external forces by a vector analyzer network to activate the sensor and identify its resonance.[7c,i,10] This approach unfortunately leads to a loss of sensitivity, undesired consumption of valuable resources of system memory, and sacrifice of signal processing rate.

Herein, we report an LC resonator-based wireless pressure sensing technology (LC-WPS) for flexible contact pressure detection. It consists of a fully flexible passive sensor and signal-reading circuitry for data processing. The passive sensor can detect the pressure signal by shifting the resonant frequency, which is correspondingly converted into a voltage change through electromagnetic coupling between the sensor and receiver coils in the circuit. Importantly, by optimizing the sensor resonant frequency and the excitation frequency of the readout circuit, we have demonstrated an outstanding sensitivity of 1.23×10^{-2} kPa^{-1} in the pressure range of 0–15 kPa and a high resolution of 54 Pa. In addition, the signal-reading circuit utilizes a single operating frequency (i.e., 13.56 MHz) without the need for frequency sweeping in practical tests, featuring fast and real-time data analysis and processing. We have successfully demonstrated human activity-monitoring applications with the LC-WPS, such as accurate and real-time perception of facial expression changes, vocalization-induced laryngeal muscle stretching, and motion-induced joint bending.

2. Results and discussion

2.1. Overall Design of the LC-WPS

Figure 1a shows the functional block diagram of the LC-based wireless pressure sensing technology, which includes two modules: 1) The flexible pressure sensor, which is equivalent to an LC resonator. It responds to an external pressure by shifting the self-resonant frequency. 2) The signal-reading circuit, which wirelessly receives the data from the sensor. It translates the shift of the self-resonant frequency into an electrical analog voltage and finally converts the voltage into a digital signal. The data can be transmitted to a portable device for post data processing and visualization according to the requirements in different application scenarios.

The communication between the flexible wireless sensor and the signal-reading circuit depends on wireless electromagnetic coupling. This design of separating the soft and hard modules greatly improves the convenience of the LC-WPS in wearable applications. Figure 1b,c presents the schematic work principle and a photo of our LC-WPS. The flexible sensor is softly attached onto the skin surface, and the circuit can be integrated with clothing such as sleeves or wristbands. The pressure signal at the sensor and skin interface is captured by the sensor and wirelessly transmitted to the flexible receiver coil and subsequently processed and transferred to the terminal electronic equipment through Bluetooth. As shown in Figure 1d, the sensor features a small size ($25 \times 10 \times 2.5$ mm^3), good flexibility and low production cost. They can be easily attached to different parts over the body to wirelessly monitor the pressure signals in real time (Figure 1e,f).

2.2. Design of the Wireless Pressure Sensor

The wireless pressure sensor consists of three layers, including the antenna layer, the deformable fabric layer, and the ferrite film (**Figure 2**a). The top antenna involves two layers of planar spiral inductive coils. The self-inductance and mutual inductance of the two coils determine the equivalent inductance value (L_t) of the antenna. The parallel capacitance between the two layers and the parasitic capacitance among conductive strips together form the equivalent capacitance (C_t). The middle layer of the sensor is an elastic fabric, which is highly resilient, flexible, and breathable. The bottom layer is a ferrite film with ultrahigh electromagnetic permeability and radiation absorption. When an external force is applied, the fabric is mechanically deformed, and the distance between the ferrite film and the antenna decreases, resulting in changes in the magnetic field around the antenna. As a result, the equivalent inductance of the sensor L_t changes. The sensor's resonant frequency f_t can be expressed in Equation (1). Therefore, the resonant frequency of the sensor changes along with the external load.

$$f_t = \frac{1}{2\pi\sqrt{L_t C_t}} \tag{1}$$

The equivalent circuit of the sensor coupled to the receiver coil is shown in Figure 2b. The excitation frequency is the same as the radio frequency identification technique of 13.56 MHz. The sensor resonant frequency is transmitted to the signal-reading circuit through the electromagnetic coupling effect and further converted into an alternating voltage (V_{out}). The LC-WPS finally outputs a direct voltage (V) by rectifying V_{out}.

According to formulas (S1-S7) in the Supporting Information, the most important variables affecting V_{out} are the coupling coefficient k and the quality factors Q_t and f_t. The design challenge is to maximize the output V_{out} by optimizing the three variables. k depends on the structure of the antenna and the relative position between the sensor and the receiver coil (i.e., to be treated as a constant because the relative location of the two elements does not change). Considering the geometrical shape and the potential slight mismatch between the antenna and receiver coils, there might be a weak coupling effect between the two components. Therefore, the value of k is likely to be small.[11] Figure 2c shows the relationship of V_{out}, Q_t and f_t as k is set as 0.1. As the resonant frequency is close to the excitation frequency (13.56 MHz, e.g., Region I), changes in both Q_t and f_t induce considerable variations in V_{out}. As f_t deviates from 13.56 MHz (e.g., Region II), the influence of Q_t and f_t on V_{out} becomes weak. Therefore, V_{out} can be maximized by matching f_t to the excitation frequency at a large Q_t value.

To verify this hypothesis, we design four types of antenna layers with different f_t values by adjusting the design parameters of the double-layer inductive coils, including the winding direction and the location of the through-hole connection. Figure 2d is a schematic diagram of the structure for the four types of antennas in sensors I, II, III, and IV. Geometric parameters are listed in Table S1 (Supporting Information). In general, the winding direction determines the equivalent inductance: as the top coil turns clockwise and the bottom coil turns anticlockwise (e.g., sensors I and III), the induced electric current generates a

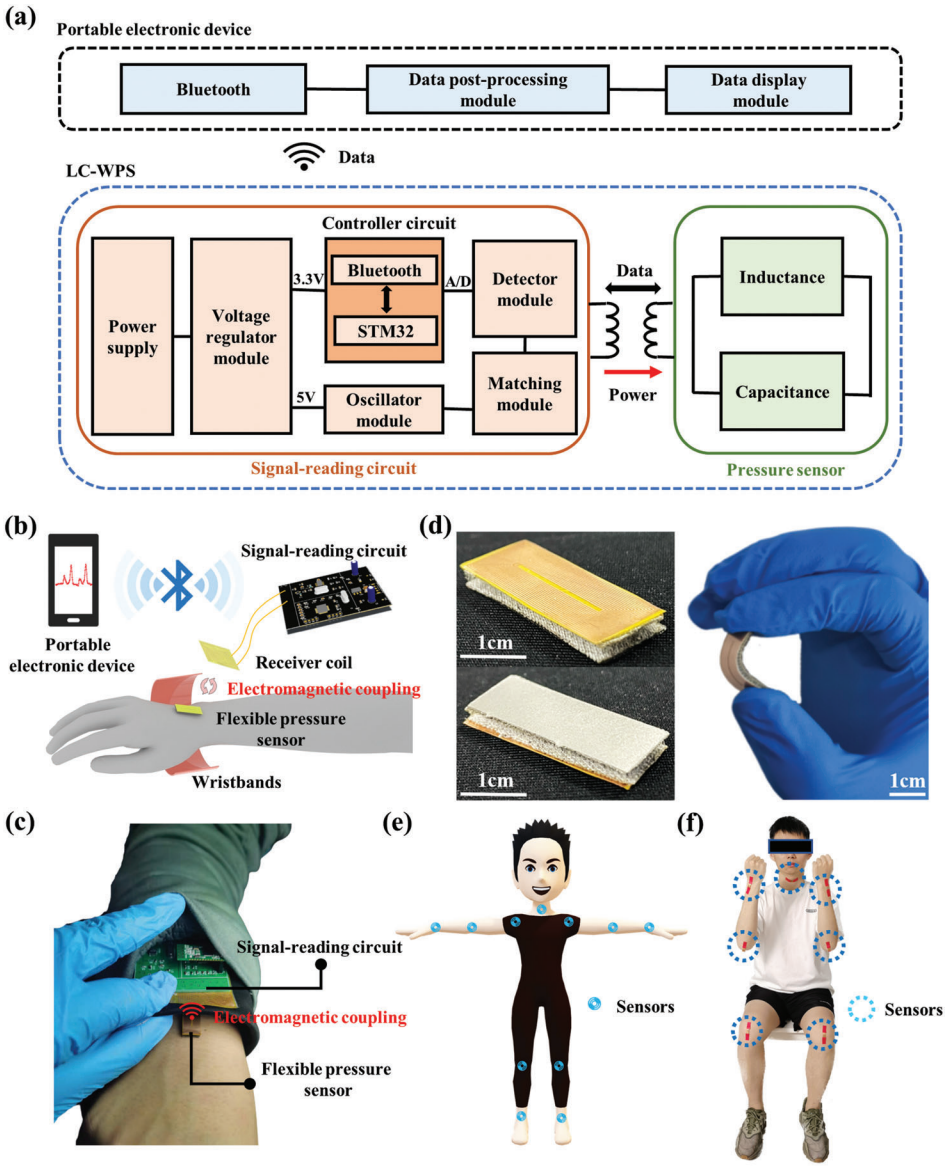

Figure 1. General introduction to the LC-WPS. a Functional block diagram showing two parts of the LC-WPS: a) wireless pressure sensor and a signal-reading circuit. It can communicate with different portable electronic devices in various application scenarios. b,c) Schematic diagram and photograph showing a volunteer wearing the LC-WPS sensor on his wrist. d) Photographs of the sensor in the top and bottom views, with one sensor highly bent. e,f) Schematic diagram and photograph of the wearable passive sensors on multiple parts of the body for motion monitoring.

magnetic field in the same direction and a large equivalent coil; as the two coils turn anticlockwise (e.g., sensors II and IV), the resonant frequency is more similar to that with a single-layer coil.[8] In addition to the winding direction, the connection site probably controls the equivalent capacitance between the two layers of coils.[12] The f_t of the four sensors is determined through the phase spectrum of the receiver coil when it is coupled with any of the four sensors individually (Figure 2e). The phase spectrum of the receiver coil itself maintains a 90° phase (inductive characteristic) at low frequencies and drops to a −90° phase (capacitive characteristic) at high frequencies, from which the self-resonant frequency of the receiver coil is 63 MHz at the zero-phase point (Figure S1, Supporting Information).

When the receiver coil is coupled with the four types of sensors, a peak appears at the resonant frequency f_t of the sensor. The convex and concave peaks located in the 90° and −90° phase regions of the receiver coil correspond to these f_ts.[13] The resonant frequencies of sensors I, II, and IV are ≈12.8, 73.1, and 72.6 MHz, respectively. Under a pressure of 40 kPa, the resonant frequencies decrease to 12.1, 66.2, and 64.7 MHz accordingly. In addition, in the entire pressure range, the Q_ts of the four sensors are in the range of 26–28. In other words, sensor I is located in region *A*, sensor II and sensor IV fall in region *B*, and they all have high Q_ts in Figure 2c. For sensor III, multiple peaks appear on the phase spectrum of the receiver coil, which can probably be attributed to the "frequency splitting" phenomenon: the

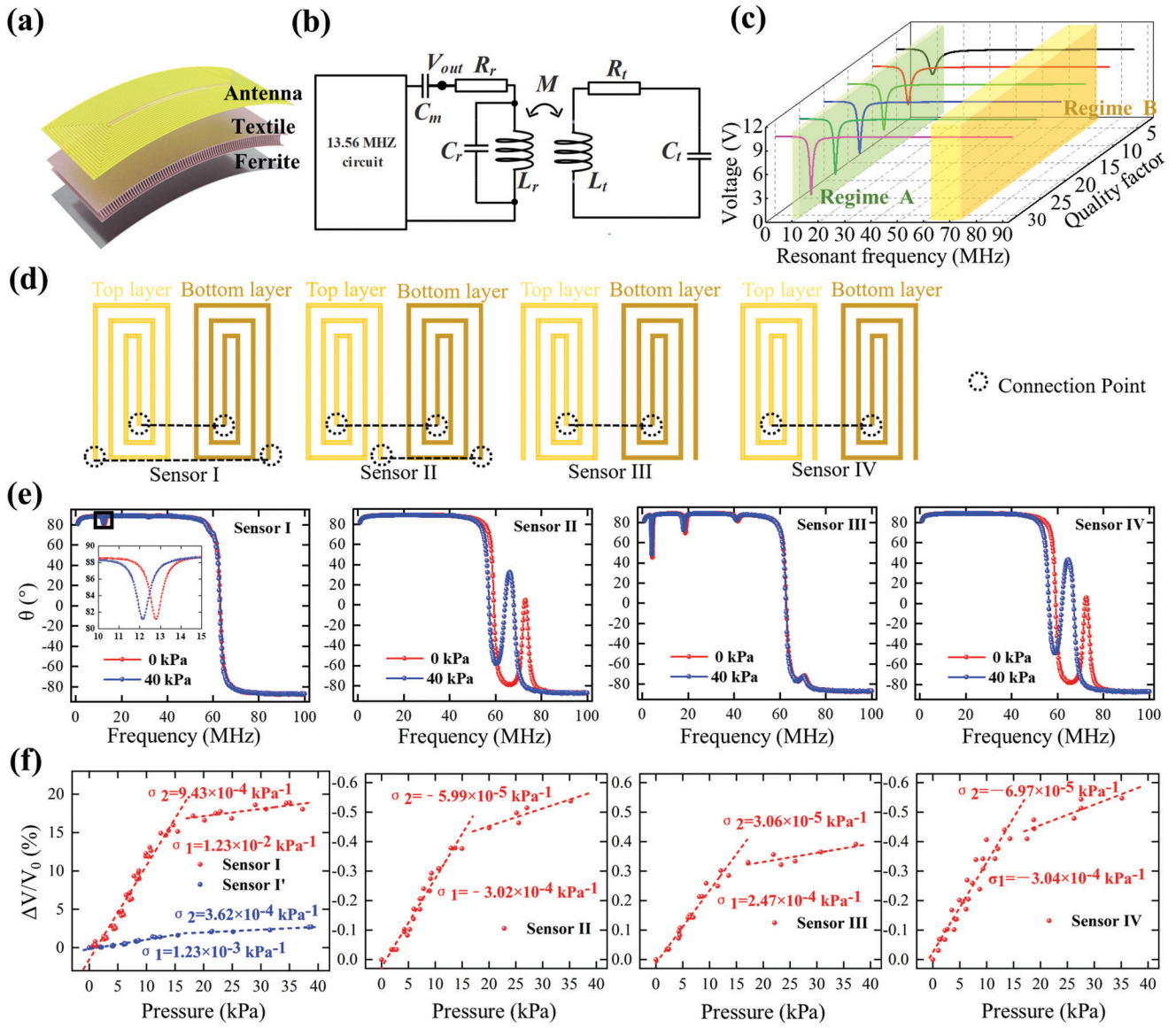

Figure 2. Design and simulation of the sensors. a) Structural model of the flexible sensor. b) Circuit model of the LC-WPS. c) Simulation results of the relationship among the output voltage of the circuit, the resonant frequency and quality factor of the sensor ($k = 0.1$). d) Schematic diagram of the coil arrangement of four types of sensors. The top and bottom coils have been laid on the same plane. e) The phase spectra of the receiver coil coupled to the four types of sensors. f) The sensitivity curves of the four sensors composed of different coil structures in Figure d at a distance of 4 mm from the receiver coil (the blue line in Figure f is the sensitivity curve of sensor I with the ferrite film replaced with aluminum foil).

current density distribution on the sensor surface suggests that sensor III has the highest current density, indicating that the coupling strength of sensor III is much greater than those of the other three sensors (Figure S2, Supporting Information). In this case, sensor III is likely to be overcoupled with the receiver coil, causing the peak transmission efficiency to split from a single frequency into multiple frequencies. As a result, the variation in each frequency is reduced, and the sensitivity is eventually attenuated.[14]

The pressure-voltage curves of the four sensors are shown in Figure 2f. The sensitivity S of the LC-WPS is defined as $d(\Delta V/V_0)/dp$. V_0 is the direct voltage output V under zero pressure, and ΔV is the V change after pressure p is applied to the sensor. In the entire sensing range (from 0 to 40 kPa), all the sensitivity curves are divided into two sections: as the pressure is below 15 kPa, the sensitivities of the four sensors are 1.23×10^{-2} kPa^{-1}, -3.02×10^{-4} kPa^{-1}, 2.47×10^{-4} kPa^{-1}, and -3.04×10^{-4} kPa^{-1}; as the pressure increases above 15 kPa, the sensitivity in each curve drops to 9.43×10^{-4} kPa^{-1}, -5.99×10^{-5} kPa^{-1}, 3.06×10^{-5} kPa^{-1}, and -6.97×10^{-5} kPa^{-1}, respectively. The sensitivity segmentation is mainly due to the mechanical properties of the elastic fabric layer (Figure S3, Supporting Information). In comparison to sensor II and sensor IV, sensor I has the highest sensitivity. This is consistent with the aforementioned speculation, i.e., the closer the self-resonant frequency of the sensor is to 13.56 MHz, the higher its sensitivity is.

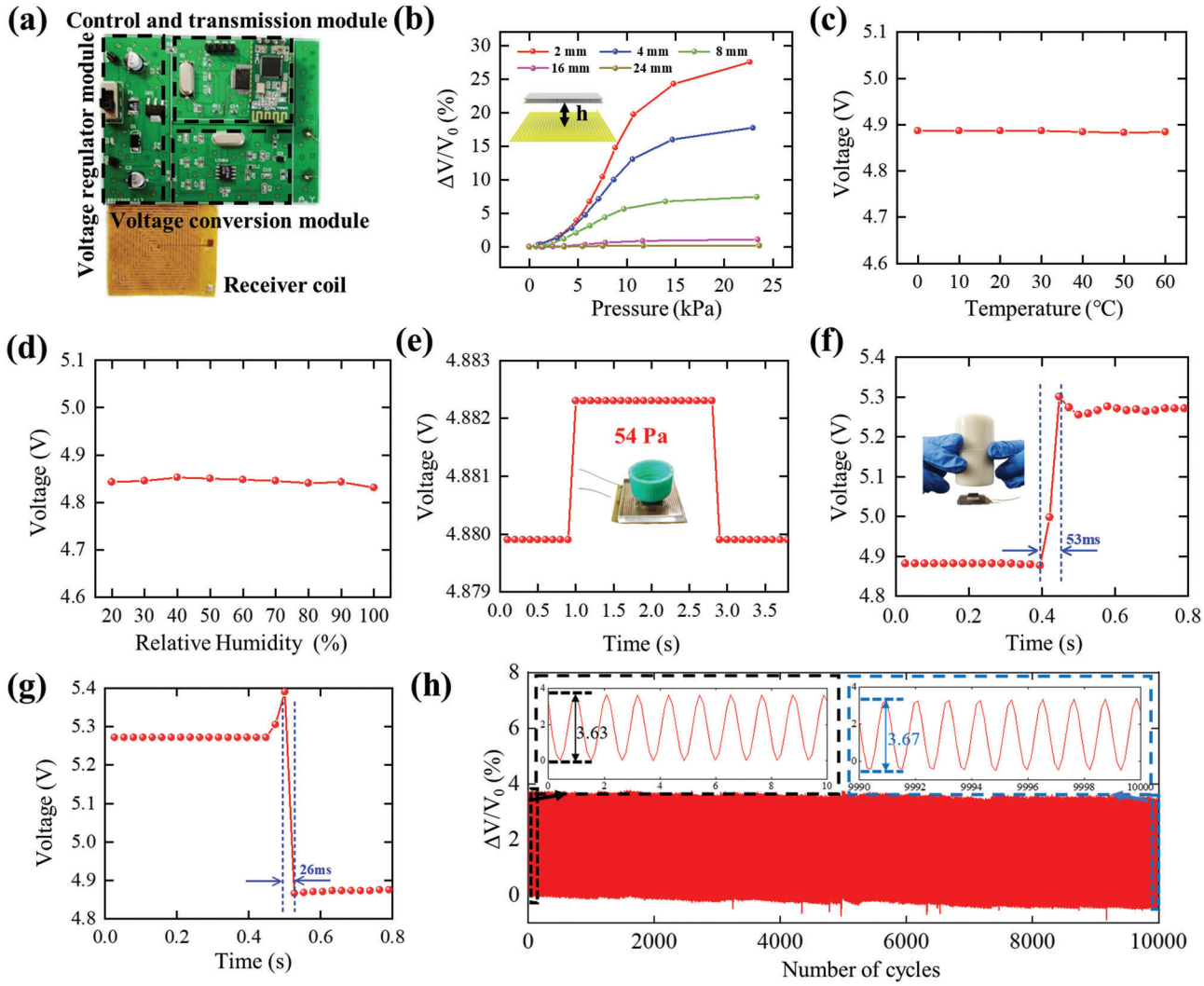

Figure 3. Performance characteristics of the wireless pressure sensor. a) Photograph of the signal-reading circuit. b) The sensitivity curves of the LC-WPS with various vertical distances *h* between the sensor and the receiver coil. c,d) Effects of the temperature and relative humidity on the output voltage. e) Time-resolved voltage responses when a pressure of 54 Pa is applied to the sensor. f) Time-resolved voltage responses when an object falls on the sensor. g) Time-resolved voltage response when the object is quickly removed. h) Time-resolved voltage in response to a cyclic load of 4.8 kPa 10000 times.

We have further explored the effect of absorbing materials on the sensitivity of the LC-WPS. In Figure 2f, the red curve and the blue curve correspond to the pressure-voltage changes when using the ferrite film and the metal aluminum film, respectively, as the absorbing material of the sensor. Obviously, the sensitivity of the sensor with the ferrite film (sensor I) is approximately ten times higher than that of the aluminum film (sensor I'). When the aluminum film is exposed to an electromagnetic field, a closed-path current is generated, which induces a second electromagnetic field and thereby reduces the original electromagnetic field strength, resulting in a decrease in the device sensitivity.[7c] The sensitivity and linear range of the LC-WPS can be improved by optimizing the material of the middle deformable layer.[15] The effect of different textile fabrics on the sensitivity of the sensor was explored (Figure S4 and S5, Supporting Information).

Figure 3a shows a photograph of the signal-reading circuit. It converts data transmitted from the sensor to the receiver coil into a real-time voltage signal. The electromagnetic coupling strength of the sensor and receiver coil largely depends on the coupling coefficient *k*, which is subjected to the relative position of the two components. Figure 3b compares the sensitivity curves under different vertical separation distances *h* between the receiver coil and the sensor. As expected, the sensitivity decreases with an increase in the separation distance *h*. The maximum achievable separation distance reaches 24 mm (the corresponding sensitivity is 1.52×10^{-4} kPa^{-1}). Additionally, we compared the sensitivity curves when the sensor and receiver coil were placed off the center (Figure S6, Supporting Information). When the geometric center distances between the sensor and the receiver coil change from 0 to 10 mm, the sensitivity drops by 65%. Figure S7 (Supporting Information) shows the sensitivity when the sensor

rotates 0°, 45°, 90°, and 135° around its center point. The rotation has a negligible effect on the overall sensitivity (less than 7% variation).

Our LC-WPS exhibits a less than 1% change in voltage output under temperatures from 0 to 60 °C and relative humidity from 20 to 100% (Figure 3c,d), indicating good resistance to environmental disturbances. Resolution is also one of the important criteria of the LC-WPS. The minimum force that can be detected is 54 Pa, which can meet the requirements for measuring a relatively fine force (Figure 3e). In addition, our LC-WPS shows good anti-interference capability (Figure S8, Supporting Information).

Figure 3f,g shows the response of the LC-WPS to a dynamic pressure of 8 kPa. According to the rising/falling edges of the time-resolved voltage curves, the LC-WPS has a relatively fast response time (53 ms) and recovery time (26 ms). The LC-WPS recovers faster, but it cannot be detected by the signal-reading circuit because of the sampling limit. Figure 3h shows the time-resolved voltage in response to a cyclic load of 4.8 kPa 10000 times. After 10000 cycles, the relative voltage change remains at approximately the same value of 3.63%, indicating good repeatability of the LC-WPS. There is a slight voltage offset of 0.45%, which is possibly attributed to an increased circuit noise of the signal-reading circuit over a long period of time (≈8000 s).

2.3. LC-WPS for Human Motion Detection

The potential utility of our LC-WPS has been demonstrated in several typical scenarios by wirelessly monitoring the pressure signals in human daily activities.

Motions of laryngeal and neck joints provide physiological cues of speaking, coughing, and exercising of the neck, which are valuable in the diagnosis and prevention of bronchitis, cervical spondylosis and other related diseases.[16] As shown in **Figure 4**a, the sensor is worn on the throat by covering a thin layer of tape on top of the sensor. When the volunteer coughs gently three times, the motions of his Adam's apple apply pressure on the sensor, correspondingly leading to three voltage pulses (Figure 4b).

Monitoring the motions of Adam's apple can also reflect the number of syllables and the volume of voice, thus potentially providing acoustic phonetics of individual speakers. For example, when the volunteer pronounces monosyllable words (such as "me", "my", "may"), disyllabic words (such as "money", "mother", "medal"), or trisyllabic words (such as "medical", "marriage" and "melody") twice at approximately the same volume, the voltage outputs of his voice messages are synchronously recorded by our LC-WPS (Figure 4c). The number and profiles of the voltage peaks are reproducible between the pronunciation repeats. They have been validated by control experiments in parallel using a commercial audio recording application (Figure 4c).

The changes in the speaker's voice volume can also be detected by our LC-WPS. In Figure 4d, when the volunteer pronounces the words "medal" and "mother" in a low and loud voice, respectively, the output voltages allow for successful differentiation of his voice volume by the peak amplitudes as the signals of his laryngeal muscle movements. In addition, two volunteers independently pronounce the words "Hi", "Made" and "Medicine" twice. As shown in Figure 4e, the individual characteristics in terms of the amplitude and rhythm of the voltage peaks can be used for identification of their speaking habits.

A long period of bowing may increase the incidence of cervical spondylosis. Appropriate exercise of the cervical spine is an effective way to prevent cervical spondylosis. We have developed an application for the cell phone and integrated it with our LC-WPS to monitor cervical spine activity. The sensor is attached to the neck, and the receiver coil is placed in the neck pillow (Figure 4f). When the volunteer does not move his neck (for example, looking down at the mobile phone) for a period of time (e.g., five minutes), our device senses no signal change. Then, a warning dialog box pops up in the app, prompting "You should exercise your neck!" (Figure S9, Supporting Information). Figure 4h shows the changes in output voltage when a volunteer bows or raises his head repeatedly. When the volunteer bows his head, the pressure on the sensor increases, and the voltage increases. When he raises the head, the pressure on the sensor decreases to a level less than the initial value, and the voltage decreases accordingly. In addition, our LC-WPS has successfully been applied for facial expression differentiation (e.g., smiling, Figure S10, Supporting Information).

A wearable interactive strategy can be achieved by monitoring the activity of hand motions.[17] **Figure 5**a shows the time-resolved voltage when the wrist bends to 30°, 60°, and 90° three times. The sensor is fixed on the wrist and wrapped with an elastic strap. When the volunteer bends his/her wrist down, the strap elastically stretches, which in turn induces pressure on the sensor and results in a voltage increment. As expected, the greater the wrist bending angle is, the larger the voltage changes. To realize an interactive system for robot control, we have further developed a circuit to receive multiple sensor data to realize multipoint force determination. The traveling trajectory of a smart robot is successfully controlled by monitoring wrist movement through the LC-WPS (Figure 5b). Two wireless sensors (sensor #A, sensor #B) were worn on the left and upper parts of the wrist and coupled to two receiver coils fixed outside of a wristband (Figure 5c). The signal-reading circuit has been worn on the arm. Figure 5d shows the images when the volunteers made gestures, such as bending up/down and turning left/right. The force exerted on the sensor not only includes the pressure caused by joint movement but also involves the tension of the wristband on the sensor caused by joint bending. Figure 5e shows the corresponding voltage outputs of the two sensors under the four gestures.

Here, we use the values of 0, 1, and −1 to represent the initial value, increase and decrease of the voltage, and control the smart car motion by the combinations of the three values. Initially, the wrist remains horizontally still, and the wristband squeezes on the wrist, inducing an initial pressure. The signal-reading circuit converts the two voltage values to state "0, 0" and sends them to the control circuit on the smart car through Bluetooth. According to the preset comment, the smart car is in a stationary state. When the wrist bends upward, the upper part of the wristband becomes wrinkled, which reduces the pressure and voltage on sensor #B. Meanwhile, the voltage of sensor #A slightly increases due to a small amount of pressure from the left side of the wristband. Therefore, the smart car moves forward (State: 1 -1). In State -1 0 or 1 0, the wrist bends to left/right, and the pressure on sensor #A decreases/increases, leading to a decrease/increase in the corresponding voltage. The smart car turns left/right. The

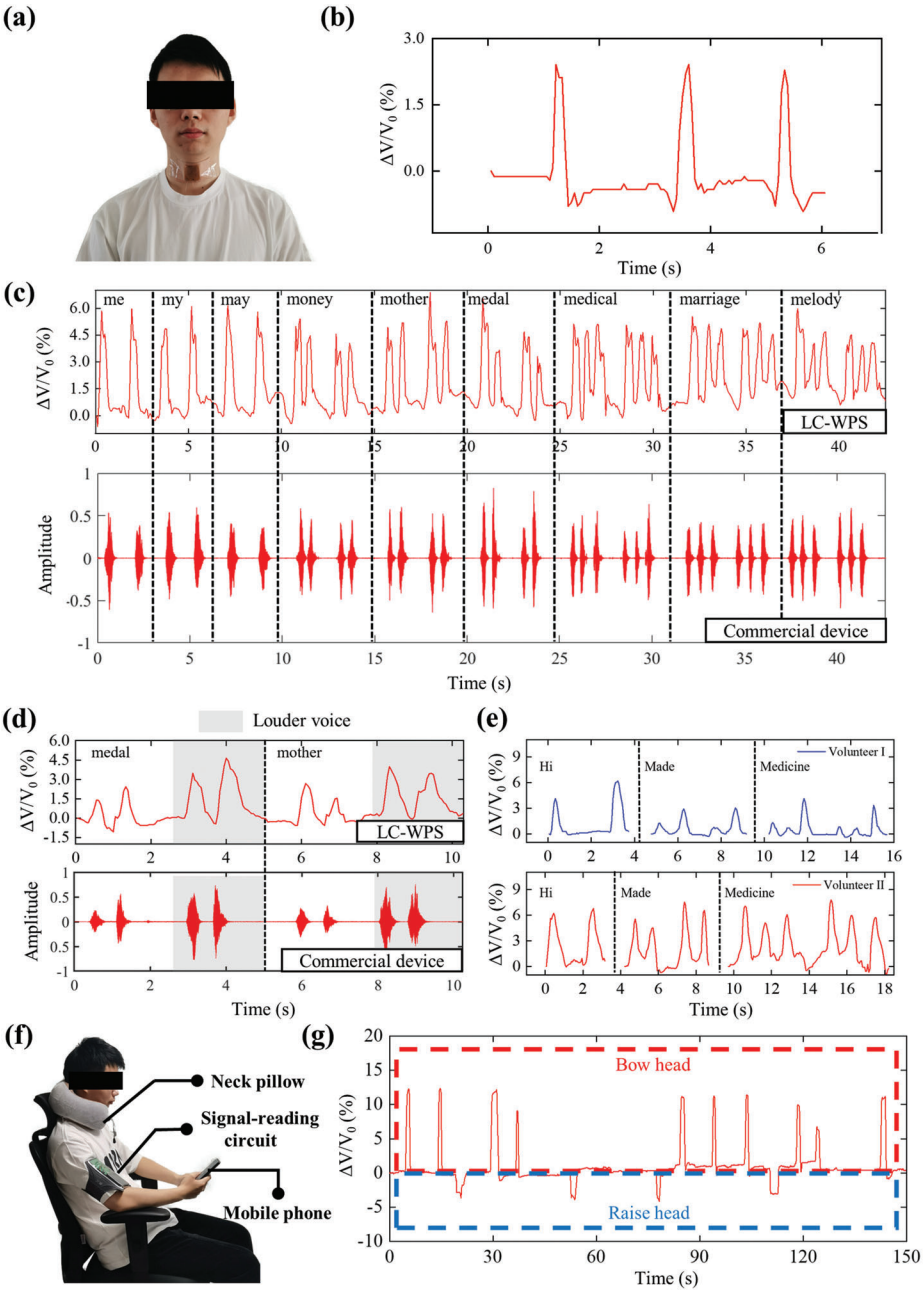

Figure 4. The LC-WPS for monitoring laryngeal and neck movements. a) Photograph of the passive sensor attached to the throat. b) Output voltage waveforms of coughing recorded by the LC-WPS. c) Time-resolved output voltage in response to laryngeal motion for the pronunciation of different words, along with the comparison to the signal recorded by a commercial audio device. d) Output voltage waveforms when the voice volume changes. e) Comparison of the output waveforms between two volunteers' pronunciations. f) Schematic diagram of applying the LC-WPS to detect the motions of the volunteer's cervical spine. g) Changes in output voltage when a volunteer bows or raises his head repeatedly.

slight voltage increment for Sensor #B is due to small pressure variations in this gesture, which can be treated as zero by setting the proper voltage threshold in the data post-processing. When the wrist bends downward, the pressure on the two sensors increases, the two voltages increase, and the smart car moves backward (State 1). For example, when the wrist bends up, the voltages are positive on sensor #A and negative on sensor #B.

In addition, the LC-WPS has shown an excellent capability in distinguishing finger touches and presses (Figure S11, Supporting Information) and detecting pulse signal changes after physical activity (Figure S12 and S13, Supporting Information). Collectively, these demonstrations with the LC-WPS allow for detecting real-time human physiological activities with a high sensitivity, showing that our LC-WPS has a wide range of application prospects in wearable medical care and sports biomechanics.

Table 1 compares our LC-WPS and several other wireless passive pressure sensing technologies. Most of the sensors with LC

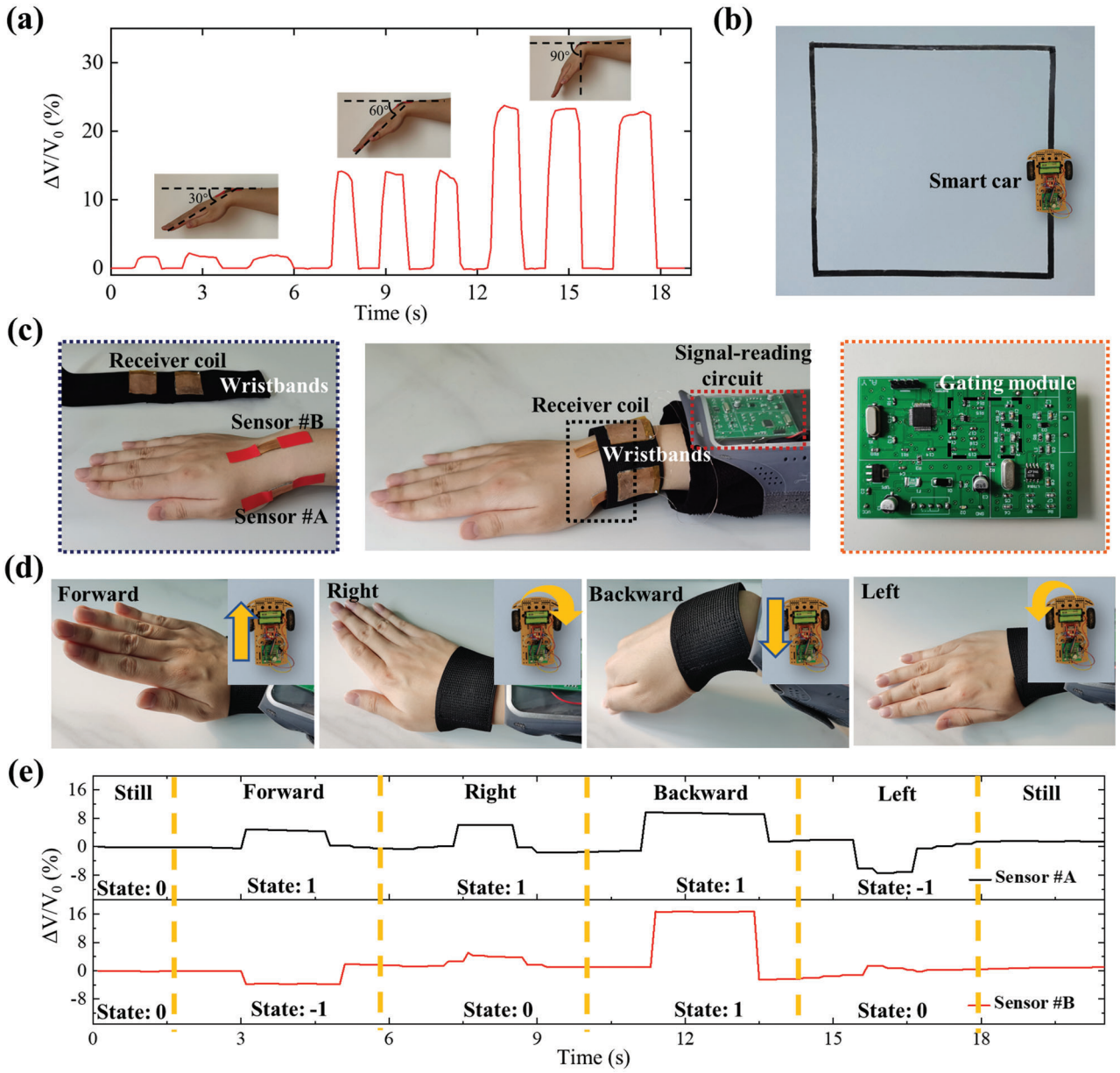

Figure 5. Monitoring hand/wrist movement through the LC-WPS. a) The time-resolved voltage when the wrist bends to 30°, 60°, and 90° three times. b) Photo of the route control experiment tested with a smart car. c) Photograph of multichannel wearable interactive system based on the LC-WPS. d) The smart car moving in different directions under different gestures. e) Output voltage waveforms when performing different hand actions.

Table 1. Comparison of the device performance of wireless pressure sensing technologies.

Reference	Sensing mechanism	Containing rigid devices	Data transmission rate [Hz]	Method of measurement	Sensitivity [kPa^{-1}]	Linear range [kPa]	Response/recovery time [ms]
[19]	Resistance	Yes	10-20	Resistance → Voltage	6×10^{-4}	0–10	–/–
[20]	Resistance	Yes	10	Resistance → Voltage	5×10^{-4}	0–500	–/–
[10b]	Capacitance	No	2	Sweeping Frequency	-2.55×10^{-4}	0–200	100/100
[7h]	Capacitance	No	–	Sweeping Frequency	-2.70×10^{-3}	0–26.7	–/–
[10c]	Capacitance-Inductance	No	5	Sweeping Frequency	-3.37×10^{-4}	0–248	1700/1700
[7c]	Inductance	No	5	Sweeping Frequency	-4.3×10^{-3}	0–20	100/100
This work	Inductance	No	38	Frequency → Voltage	1.23×10^{-2}	0–15	53/26

resonators in the literature show pressure-induced changes in inductance or capacitance, which are eventually converted into the output of resonant frequency.[7c,h,10c,18] However, this strategy needs to determine the resonant frequency of the sensor by sweeping the amplitude/phase spectrum of the receiver coil with a vector analyzer network, thus limiting highly sensitive, fast and real-time detection. The previous reports of[19] and[20] implemented real-time processing and display, but they relied on rigid chips in their sensor systems, sacrificing flexibility to some extent. In contrast, our LC-WPS not only realizes real-time data acquisition, processing and display with a high sensitivity but also fully separates the flexible sensor and the rigid circuit, achieving a rigid chip-free wireless sensing interface. This feature potentially allows for fast data acquisition with high sensitivity and wearable comfort in the demonstration of utility in human motion detection.

A similar strategy has been proposed by implementing a resistive strain sensor in the LC architecture.[9] The work focuses on maximizing the strain-induced voltage output in a low-Q_t. (in the range of 1–10) LC platform.[9] In contrast, the LC-WPS in this manuscript presents a distinct solution to enhance the sensitivity (i.e., pressure-to-voltage) in a high-Q_t (>25) LC structure. Our strategy proposes design criteria in the high-Q_t situation and greatly expands the application scope of LC-based passive sensing technology with Q_t in different ranges.

3. Conclusions

A wireless flexible pressure sensing technology based on an LC resonator has been developed for human motion detection. By matching the resonant frequency of the sensor and the operating frequency of the circuit, we can maximize the changes in the resonant frequency with a high sensitivity of 1.23×10^{-2} kPa^{-1} within the pressure range of 0–15 kPa. Distinct from previous reports, the proposed sensing technology processes data in a real-time manner by using a single operating frequency, presenting high wearability and portability. In addition, it exhibits great reproducibility and stability under environmental temperature and humidity fluctuations. It has been implemented in several applications for human body motion detection, including movement detection of the larynx, cervical spine and wrist. Therefore, the LC-WPS provides a promising platform for wireless tactile sensing, particularly for emerging wearable electronics.

4. Experimental Section

Fabrication of the Wireless Pressure Sensor: The device was designed with 3D drawing software (AutoCAD, Autodesk), including four double-layer planar spiral inductors with different geometrical parameters. It was fabricated by standard screen printing and etching to pattern the copper electrodes on both sides of a polyimide film (25 μm thick). The through-hole connections were created by the electroplating technique. A polyimide film with a thin layer of adhesive was covered on each copper side. Four types of LC antenna layers were built in this step. In the second step, laser micromachining was employed to trim the geometrical shape of the ferrite films (Nanjing Advanced Magnetic Material, Co., Ltd.), the antennas, the fabric layer (Suzhou Haoke Textile, Co., Ltd.) and double-sided tape (467 MP, 3 M). Finally, the flexible wireless pressure sensor was assembled by aligning the ferrite film, LC antenna, fabric layer and double-sided tape according to the alignment markers.

Design of the Signal-Reading Circuit: The signal-reading circuit was composed of 1) a power supply modulus, 2) a voltage regulator module to stabilize the voltage provided by the power supply, 3) an oscillator module to drive the receiver coil, 4) a matching module to improve the transmission efficiency of the circuit, 5) a detector module to convert the high-frequency alternating current signal into a low-frequency direct current signal, 6) an STM 32-based microcontroller, and 7) a Bluetooth module to collect, process and transmit data.

Characterization of the Sensitivity of the LC-WPS: A custom calibration system was used to evaluate the overall sensitivity. The calibration system consisted of a linear displacement stage (LTS300/m, Thorlabs, Inc.) with a motion resolution of 0.1 μm, a force gauge (M5-2, Mark-10, Corp.) with a resolution of 10 mN, and the signal-reading circuit as aforementioned. A desktop computer was used to control the movement of the linear displacement stage, and the force applied on the sensor was recorded by the force gauge. The pressure received by the sensor was defined as the ratio of the force to the contact area of the sensor. Each pressure correspondingly results in an output voltage, which was read out by the signal-reading circuit.

Assessments on the Environmental Factors: To assess the influence of the environmental temperature variations, the sensor was placed over a hot plate with a distance of 30 cm, and an infrared thermometer is used to measure the temperature of the sensor surface. To characterize the humidity influence, the sensor was placed in an airtight container with a small opening. The humidity inside the container was controlled by a humidifier, and the ambient humidity was measured with a commercial hygrometer. The output voltages of the LC-WPS were recorded along with the changes in environmental temperature/humidity.

Evaluation of the Response/Recovery Time: The response/recovery time of the sensor was evaluated through the free falling strategy. Specifically, a two-kilogram object was released vertically above the sensor at a distance of 5 cm. According to the gravitational acceleration formula, the speed at which the weight falls on the sensor is 0.99 m s^{-1}, and the time interval during which the object touches the sensor surface until it fully stops is 24 ms. The response time of the sensor was calculated from the period where the output voltage step occurs. Similarly, the recovery time was determined once the heavy object is quickly moved away from the sensor. The sampling frequency of the output voltage was 38 Hz.

Ethics of Human Motion Detection by LC-WPS: On-skin experiments for human motion detection by LC-WPS were conducted according to the protocol which were approved by the Committee on Ethics of Human Specimens and Animal Experiments at Soochow University. Informed written consent of all the participants involved in the experiments was obtained.

Construction and Testing of a Smart Car: The overall dimensions of the smart car were 21 cm × 16 cm × 8 cm (length × width × height, ElecFans, Co.). The main control chip in the smart car was STM32F103RBT6. Bluetooth technology was adopted to communicate with the LC-WPS. Two front wheels were equipped with deceleration motors, and the rear wheels were universal wheels. By setting the command in advance in the control circuit of the electric car, the trajectory of the electric car corresponds to the two voltage signals of the LC-WPS. The sensors were fixed on the two sites of the wrist, and a wristband was wrapped around the joint.

Supporting Information

Supporting Information is available from the Wiley Online Library or from the author.

Acknowledgements

This work was supported by the National Natural Science Foundation of China under Grant No. 61601317, The Natural Science Foundation of the Jiangsu Higher Education Institutions of China (20KJB510001), Natural Science Foundation of Jiangsu Province of China (BK20211308), the 111 project, Joint International Research Laboratory of Carbon-Based

Materials and Devices, the Collaborative Innovation Center of Suzhou Nano Science, and Suzhou Key Laboratory of Nanotechnology and Biomedicine.

Conflict of Interest

The authors declare no conflict of interest.

Data Availability Statement

The data that support the findings of this study are available from the corresponding author upon reasonable request.

Keywords

human motion detections, LC resonators, pressure sensors, wireless electrical circuitry

Received: November 14, 2022
Revised: March 20, 2023
Published online: May 5, 2023

[1] a) S. Chen, Y. Wang, L. Yang, F. Karouta, K. Sun, *Nano-Micro Lett.* **2020**, *12*, 136; b) Q. Liu, Y. Liu, J. Shi, Z. Liu, Q. Wang, C. F. Guo, *Nano-Micro Lett.* **2021**, *14*, 21; c) H. Zhang, D. Liu, J. H. Lee, H. Chen, E. Kim, X. Shen, Q. Zheng, J. Yang, J. K. Kim, *Nano-Micro Lett.* **2021**, *13*, 122; d) M. Lin, Z. Zheng, L. Yang, M. Luo, L. Fu, B. Lin, C. Xu, *Adv. Mater.* **2022**, *34*, 2107309; e) T. R. Ray, J. Choi, A. J. Bandodkar, S. Krishnan, P. Gutruf, L. Tian, R. Ghaffari, J. A. Rogers, *Chem. Rev.* **2019**, *119*, 5461.

[2] a) H. Wen, C. Chen, S. Li, Y. Shi, H. Wang, W. Guo, X. Liu, *Small Methods* **2021**, *5*, 2001055; b) K. S. Chun, Y. J. Kang, J. Y. Lee, M. Nguyen, B. Lee, R. Lee, H. H. Jo, E. Allen, H. Chen, J. Kim, L. Yu, X. Ni, K. Lee, H. Jeong, J. Lee, Y. Park, H. U. Chung, A. W. Li, P. A. Lio, A. F. Yang, A. B. Fishbein, A. S. Paller, J. A. Rogers, S. Xu, *Sci. Adv.* **2021**, *7*, eabf9405; c) P. Escobedo, M. D. Fernández-Ramos, N. López-Ruiz, O. Moyano-Rodríguez, A. Martínez-Olmos, I. M. Pérez de Vargas-Sansalvador, M. A. Carvajal, L. F. Capitán-Vallvey, A. J. Palma, *Nat. Commun.* **2022**, *13*, 72; d) G. Wu, I. Heck, N. Zhang, G. Phaup, X. Zhang, Y. Wu, D. E. Stalla, Z. Weng, H. Sun, H. Li, Z. Zhang, S. Ding, D.-P. Li, Y. Zhang, *Sci. Adv.* **2022**, *8*, eabn2277.

[3] W. Gao, S. Emaminejad, H. Nyein, S. Challa, K. Chen, A. Peck, H. M. Fahad, H. Ota, H. Shiraki, D. Kiriya, *Nature* **2016**, *529*, 509.

[4] a) Y. Yu, J. Nassar, C. Xu, J. Min, Y. Yang, A. Dai, R. Doshi, A. Huang, Y. Song, R. Gehlhar, A. D. Ames, W. Gao, *Sci Robot* **2020**, *5*, eaaz7946; b) Y. Park, K. Kwon, S. S. Kwak, D. S. Yang, J. A. Rogers, *Sci. Adv.* **2020**, *6*, eabe1655; c) Y. Song, J. Min, Y. Yu, H. Wang, Y. Yang, H. Zhang, W. Gao, *Sci. Adv.* **2020**, *6*, eaay9842; d) X. Liu, C. Tang, X. H. Du, S. A. Xiong, S. Y. Xi, Y. F. Liu, X. Shen, Q. B. Zheng, Z. Y. Wang, Y. Wu, A. Horner, J. K. Kim, *Mater. Horiz.* **2017**, *4*, 477.

[5] H. U. Chung, B. H. Kim, J. Y. Lee, J. Lee, Z. Xie, E. Ibler, K. Lee, A. Banks, J. Jeong, J. Kim, C. Ogle, D. Grande, Y. Yu, H. Jang, P. Assem, D. Ryu, J. Kwak, M. Namkoong, J. Park, J. Rogers, *Science* **2019**, *363*, eaau0780.

[6] a) S. Han, J. Kim, S. M. Won, Y. Ma, D. Kang, Z. Xie, K. T. Lee, H. U. Chung, A. Banks, S. Min, *Sci. Transl. Med.* **2018**, *10*, eaan4950; b) R. Z. Lin, H. J. Kim, S. Achavananthadith, S. A. Kurt, S. C. C. Tan, H. C. Yao, B. C. K. Tee, J. K. W. Lee, J. S. Ho, *Nat. Commun.* **2020**, 11; c) L. Xu, Z. Liu, X. Chen, R. Sun, Y. Li, *Adv. Intell. Syst.* **2019**, 1900056; d) D. P. Rose, M. E. Ratterman, D. K. Griffin, L. Hou, N. Kelley-Loughnane, R. R. Naik, J. A. Hagen, I. Papautsky, J. C. Heikenfeld, *IEEE Trans. Biomed. Eng.* **2015**, *62*, 1457.

[7] a) Y. Huang, D. Fang, C. Wu, W. Wang, X. Guo, P. Liu, *Rev. Sci. Instrum.* **2016**, *87*, 065007; b) H. Kou, L. Zhang, Q. Tan, G. Liu, W. Lv, F. Lu, H. Dong, J. Xiong, *Sens. Actuator A-Phys.* **2018**, *277*, 150; c) B. Nie, R. Huang, T. Yao, Y. Zhang, Y. Miao, C. Liu, J. Liu, X. Chen, *Adv. Funct. Mater.* **2019**, *29*, 1808786; d) J. Kim, M. Kim, M.-S. Lee, K. Kim, S. Ji, Y.-T. Kim, J. Park, K. Na, K.-H. Bae, H. Kyun Kim, F. Bien, C. Young Lee, J.-U. Park, *Nat. Commun.* **2017**, *8*, 14997; e) Q. Huang, L. Dong, L. Wang, *J. Microelectromech. Syst.* **2016**, *25*, 822; f) Y. Liang, M. Ma, F. Zhang, F. Liu, Z. Liu, D. Wang, Y. Li, *Sensors* **2019**, *19*, 1189; g) Q. Tan, T. Luo, T. Wei, J. Liu, L. Lin, J. Xiong, *J. Microelectromech. Syst.* **2017**, *26*, 351; h) W. J. Deng, L. F. Wang, L. Dong, Q. A. Huang, *IEEE Sens. J.* **2018**, *18*, 4886; i) R. Nopper, R. Has, L. Reindl, *IEEE Trans. Instrum. Meas.* **2011**, *60*, 2976.

[8] C. M. Boutry, L. Beker, Y. Kaizawa, C. Vassos, H. Tran, A. C. Hinckley, R. Pfattner, S. Niu, J. Li, J. Claverie, Z. Wang, J. Chang, P. M. Fox, Z. Bao, *Nat Biomed Eng* **2019**, *3*, 47.

[9] S. Niu, N. Matsuhisa, L. Beker, J. X. Li, S. Wang, J. Wang, Y. Jiang, X. Yan, Y. Yun, W. Burnetts, A. S. Y. Poon, J. B. H. Tok, X. Chen, Z. Bao, *Nat. Electron.* **2019**, *2*, 361.

[10] a) J. Coosemans, M. Catrysse, R. Puers, *Sens. Actuator A-Phys.* **2004**, *110*, 432; b) P. Wang, P. Liu, H. Feng, Y. Li, Q. Zhang, R. Hu, C. Liu, K. Xing, A. Song, X. Yang, Y. Huang, *Adv. Mater. Technol.* **2022**, *7*, 2101385; c) K. Wang, F. Lin, D. T. Lai, S. Gong, B. Kibret, M. A. Ali, M. R. Yuce, W. Cheng, *Nanoscale* **2021**, *13*, 3957.

[11] C. M. Zierhofer, E. S. Hochmair, *IEEE Trans. Biomed. Eng.* **1996**, *43*, 708.

[12] G. Qin, L. Yang, W. Lou, H. Dong, S. Yu, *Dianzi Qijian* **2021**, *44*, 773.

[13] P. J. Chen, D. C. Rodger, S. Saati, M. S. Humayun, Y. C. Tai, *J. Microelectromech. Syst.* **2008**, *17*, 1342.

[14] D. Lei, L. F. Wang, Z. Cong, Q. A. Huang, *IEEE Trans Circuits Syst I Regul Pap* **2017**, *63*, 1426.

[15] a) Z. Hui, P. Wang, J. Yang, J. Zhou, W. Huang, G. Sun, *Adv. Mater. Interfaces* **2022**, *9*, 2200261; b) Z. Hui, R. Chen, J. Chang, Y. Gong, X. Zhang, H. Xu, Y. Sun, Y. Zhao, L. Wang, R. Zhou, F. Ju, Q. Chen, J. Zhou, J. An, G. Sun, W. Huang, *ACS Appl. Mater. Interfaces* **2020**, *12*, 12155; c) H. Wang, R. Zhou, D. Li, L. Zhang, G. Ren, L. Wang, J. Liu, D. Wang, Z. Tang, G. Lu, G. Sun, H.-D. Yu, W. Huang, *ACS Nano* **2021**, *15*, 9690.

[16] a) Y. Hong, B. Wang, W. Lin, L. Jin, S. Liu, X. Luo, J. Pan, W. Wang, Z. Yang, *Sci. Adv.* **2021**, *7*; b) T. Otoshi, T. Nagano, S. Izumi, D. Hazama, N. Katsurada, M. Yamamoto, M. Tachihara, K. Kobayashi, Y. Nishimura, *Sci. Rep.* **2021**, *11*, 9973.

[17] Y. Liu, C. Yiu, Z. Song, Y. Huang, K. Yao, T. Wong, J. Zhou, L. Zhao, X. Huang, S. K. Nejad, M. Wu, D. Li, J. He, X. Guo, J. Yu, X. Feng, Z. Xie, X. Yu, *Sci. Adv.* **2022**, *8*, eabl6700.

[18] A. Palmroth, T. Salpavaara, J. Lekkala, M. Kellomäki, *Adv. Mater. Technol.* **2019**, *4*, 1900428.

[19] Y. S. Oh, J.-H. Kim, Z. Xie, S. Cho, H. Han, S. W. Jeon, M. Park, M. Namkoong, R. Avila, Z. Song, S.-U. Lee, K. Ko, J. Lee, J.-S. Lee, W. G. Min, B.-J. Lee, M. Choi, H. U. Chung, J. Kim, M. Han, J. Koo, Y. S. Choi, S. S. Kwak, S. B. Kim, J. Kim, J. Choi, C.-M. Kang, J. U. Kim, K. Kwon, S. M. Won, et al., *Nat. Commun.* **2021**, *12*, 5008.

[20] J. W. Kwak, M. Han, Z. Xie, H. U. Chung, J. Y. Lee, R. Avila, J. Yohay, X. Chen, C. Liang, M. Patel, I. Jung, J. Kim, M. Namkoong, K. Kwon, X. Guo, C. Ogle, D. Grande, D. Ryu, D. H. Kim, S. Madhvapathy, C. Liu, D. S. Yang, Y. Park, R. Caldwell, A. Banks, S. Xu, Y. Huang, S. Fatone, J. A. Rogers, *Sci. Transl. Med.* **2020**, *12*, eabc4327.